The role of mesoscale kinetic energy in phytoplankton blooms and organic carbon export in the Southern Ocean

Alexander R. Davies [*], **Fabrice Veron** [*], **and Matthew J. Oliver** [†]

[*]School of Marine Science and Policy, University of Delaware, Newark, DE, USA, and [†]School of Marine Science and Policy, University of Delaware, Lewes, DE, USA

Submitted to Proceedings of the National Academy of Sciences of the United States of America

The biological pump is an important aspect of the carbon cycle. Phytoplankton blooms in the surface ocean draw down atmospheric carbon dioxide and package it as organic particulates that sink into the deep ocean, where carbon can be sequestered on millennial timescales[1]. Mechanisms for bloom formation include episodic nutrient supply[2, 3, 4, 5], changes in light exposure due to mixing[6, 7, 8], and grazing relaxation[9]. The Southern Ocean is an iron limited[10, 11, 12], high nitrate, low chlorophyll region that draws considerable attention as a potential site for carbon drawdown through iron fertilization. However, there are no prolonged in-situ observations of the mechanisms driving naturally occurring blooms in this region. Here we show results from a biofloat that measured the development and export of a naturally occurring phytoplankton bloom in the Drake Passage. Our observations indicate low levels of mesoscale kinetic energy are necessary for bloom onset, which is confirmed by satellite observations. Post-bloom high mesoscale kinetic energy appears to facilitate bloom export to the deep ocean by changing the neutral density depths of aggregated cells. We suggest that low mesoscale kinetic energy is a precondition for bloom formation in the Drake Passage before other potentially limiting factors become significant. If mesoscale kinetic energy imposes a limitation on phytoplankton concentrations, there may be regions of the Southern Ocean unsuitable for geoengineered draw down of atmospheric carbon dioxide through large scale iron additions.

biogeochemistry | mesoscale kinetic energy | iron hypothesis | biological pump

The Southern Ocean (SO) accounts for up to 25% of total ocean carbon uptake[13, 14]. Fluxes of atmospheric carbon dioxide (CO_2) across the air-sea interface occur on relatively short timescales; the turnover time for atmospheric CO_2 in the surface ocean is on the order of one to ten years. In contrast, the deep ocean can sequester carbon on the order of 100–1,000 years[1], making it an important reservoir in the global carbon cycle. The pycnocline (a region rapidly changing density with depth) acts to prohibit vertical exchanges between the surface and deep ocean, and hence the long term, deep ocean sequestration of atmospheric CO_2.

An important mechanism for overcoming the pycnocline is biological carbon uptake and sequestration (the biological pump). Phytoplankton blooms occur in the well lit, nutrient rich regions of the surface ocean and convert CO_2 into organic carbon through oxygenic photosynthesis. If not respired by other trophic levels, phytoplankton blooms senesce, aggregate by cell-to-cell coalescence or in zooplankton fecal pellets, and sink into the deep ocean. In the deep ocean, phytoplankton are converted back to dissolved inorganic CO_2 through microbial decomposition or reach the ocean floor sediment where they are buried[1]. As Earth continues to warm[15], the biological pump in the SO is expected to play a more important role in deep ocean carbon sequestration over the coming century[16].

The standing stock of phytoplankton in the open SO is characterized by patchy, intense blooms within an otherwise unproductive[17, 18] and seasonally light limited[19] environment. Artificial fertilization experiments[12, 20, 21, 22] have shown iron to be a limiting micro-nutrient of phytoplankton blooms across the SO, which has become a potential site for augmenting the export of atmospheric CO_2 to the deep ocean through iron fertilization[23].

It is widely assumed that either seasonal or episodic mixing impacts the availability of both light and nutrients to phytoplankton. However there are no coincident in-situ observations that quantify the relationship between mesoscale kinetic energy and naturally occurring phytoplankton blooms in the SO. In this study, we investigate the SO mesoscale dynamics that implicitly control phytoplankton residence time in the euphotic layer and therefore influence the formation and senescence of naturally occurring phytoplankton blooms.

Results and Discussion

An Autonomous Profiling EXplorer (APEX float) was deployed in the Drake Passage on December 18, 2012 at 64.813° W and 59.870° S. The float collected data by profiling the water column from 2,000 dbar ($\sim$ 2,000 m) to the surface every two days between January 10 and June 4, 2013 (herein the observation period). Figure (1) shows the float trajectory. The fast, two-day profiling cycle allowed the float to act as a near-Lagrangian tracer with respect to the surface ocean motion (see Materials and Methods, Movie S1). This profiling frequency resolved mesoscale processes that have an energy peak on the order of 10 days and 100 km in the SO[24].

Significance

Artificial iron fertilization experiments have confirmed that the ability of high nitrate, low chlorophyll regions in the Southern Ocean to draw down atmospheric carbon dioxide is limited by iron availability. Hence, the Southern Ocean is a potential site for geoengineered atmospheric carbon drawdown. Here we present observations from an APEX biofloat that reveal the development and export of a naturally occurring phytoplankton bloom. Our results suggests that low levels of mesoscale kinetic energy are a necessary condition for bloom formation in the Southern Ocean while subsequent high levels of mesoscale kinetic energy appear to facilitate carbon export. We believe this precondition has been overlooked, since most successful Southern Ocean iron fertilization experiments occurred in low kinetic energy environments.

Reserved for Publication Footnotes

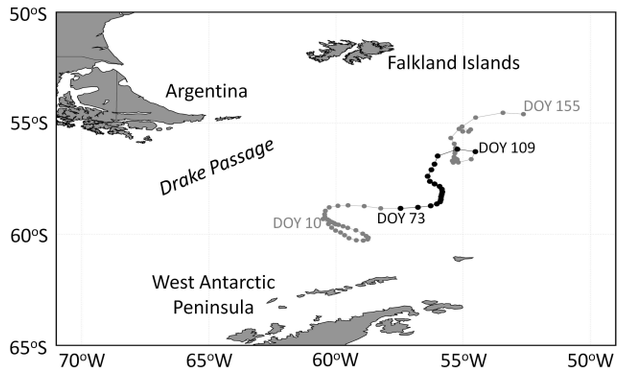

Fig. 1. The biofloat profiled the water column from ∼2,000 m to the surface every-other day. The trajectory during the observational period (DOY 10–155) is plotted in gray with the bloom-export period (DOY 93–109) in black.

The float is a "biofloat" because it measured vertical profiles of pressure, temperature, salinity, optical backscatter, colored dissolved organic matter (CDOM) fluorescence, and chlorophyll-a fluorescence. Figures (2a) and (2b) show observations of chlorophyll-a concentration ($[Chl]$, a proxy for phytoplankton abundance) and density (ρ) in the upper 500 m of the ocean (Figures S1a-d show temperature, salinity, particle backscatter and CDOM observations). To the authors' knowledge, these are the first reported observations from a biofloat operating continuously on a two-day profiling cycle in the SO.

In Figure (2a), the phytoplankton biomass is most abundant in the upper 100 m where there is sufficient light for net growth. Because the biofloat nearly tracks the motion of the surface ocean (Movie S1, Figure S2), we observe the temporal development of a phytoplankton bloom beginning on day of year (DOY) 75. The bloom persists for ∼ 20 days (which is on the order of mesoscale processes in the SO[24]) with the peak bloom between DOY 85–89. After the naturally occurring bloom, organic carbon export is observed with peak export on DOY 105.

For our analysis, we chose $\rho = 1027.45\,\mathrm{kg\,m^{-3}}$ as the characteristic isopycnal for the upper ocean, rather than the mixed layer depth (MLD). The depth of this isopyncal (z_c) is highly correlated with the depths of surrounding isopycnals and tracks the deepest extent of the surface chlorophyll layer (Figure 2a). This makes z_c a reasonable depth bound for depth integrating chlorophyll concentrations (see Materials and Methods).

Natural Bloom Sequence. The development of a phytoplankton bloom requires phytoplankton growth to outweigh losses due to respiration, sinking, or grazing. This occurs by increasing access to limiting nutrients[2, 3, 4, 5], relaxing potential losses like grazing[9], or changing residence time in the euphotic layer on seasonal[8] or turbulent[6, 7] scales. Residence time in the euphotic layer has been approximated by the MLD[9, 8], however parameterizing upper ocean dynamics with the MLD may overlook critical surface ocean mixing processes that facilitate bloom formation[7]. Here we examine the role of mesoscale ocean dynamics in naturally occurring phytoplankton bloom formation in the SO.

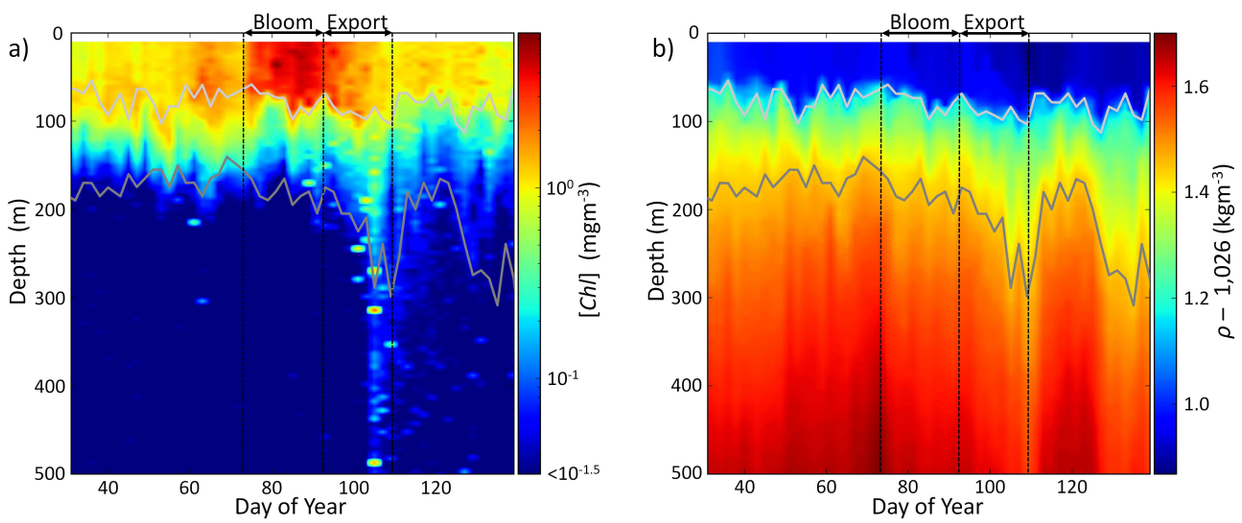

Fig. 2. *a)* Chlorophyll-a concentration ($[Chl]$) and *b)* density (ρ) observations from 500 m to surface, between DOY 31–139. The biofloat resolved mesoscale dynamics in the surface ocean, including the temporal progression of a naturally occurring phytoplankton bloom and export event (labeled). The mixed layer depth (light gray) remained fairly consistent during the observational period while the depth of the characteristic isopycnal (z_c, dark gray) deepended during export, indicating a change in the vertical structure of the surface ocean water column. We chose $\rho = 1027.45\,\mathrm{kg\,m^{-3}}$ as the characteristic isopycnal for the upper ocean (see Materials and Methods).

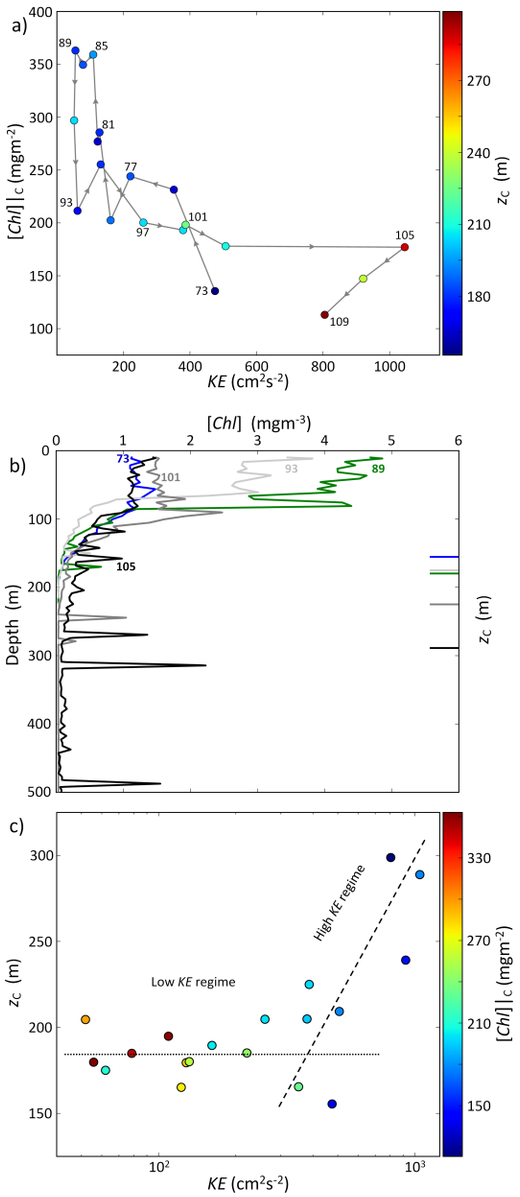

Fig. 3. *a)* The temporal progression of the depth integrated chlorophyll-a concentration ($[Chl]|_c$) with respect to mesoscale kinetic energy (KE). The sequence shows a developing bloom during low KE (DOY 73–89), phytoplankton loss likely due to ecosystem respiration and grazing (DOY 89–93), slow dilution corresponding to an increase in KE and deepening of the characteristic isopycnal (DOY 93–105), and organic carbon export into the deep ocean (DOY 101–109). *b)* Chlorophyll-a concentration ($[Chl]$) profiles show the peak bloom on DOY 89 is followed by peak carbon export between DOY 101–105. Horizontal marks on the right, vertical axis show the depth of the characteristic isopyncal (z_c) corresponding to each $[Chl]$ profile (coordinating colors). z_c deepened during peak export as *c)* KE appeared strong enough to impact the vertical structure of the water column (low KE seemingly does not impact the vertical structure).

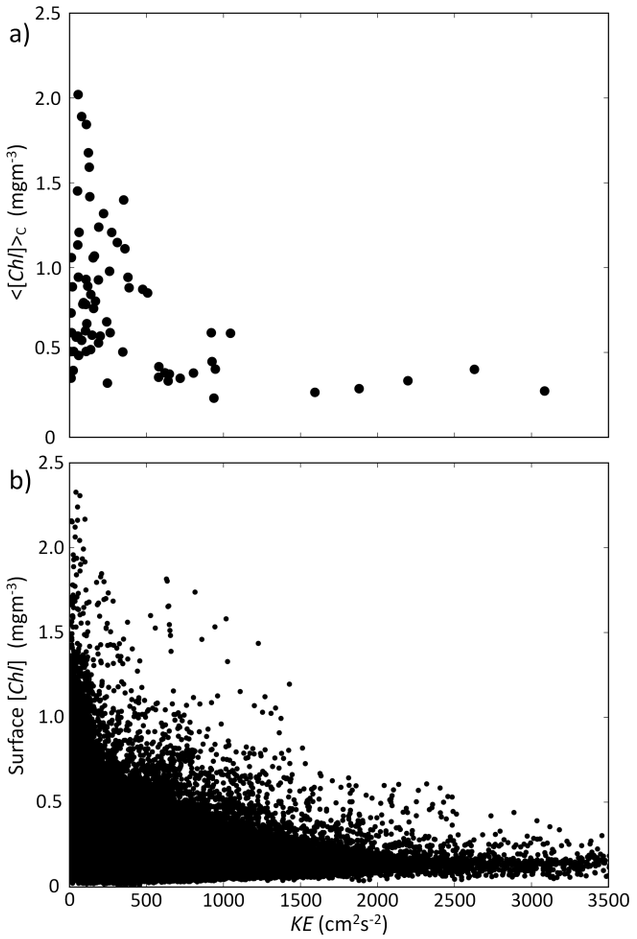

Fig. 4. *a)* The depth averaged chlorophyll-a concentration above z_c observed from the biofloat ($<Chl>_c$) is plotted with respect to NOAA OSCAR kinetic energy (KE). Our in-situ observations suggest low KE is a necessary but not sufficient condition for phytoplankton blooms, while high KE limits blooms. *b)* To test applicability of these relationships across the Drake Passage, MODIS Aqua five-day composite surface chlorophyll-a concentrations (Surface $[Chl]$) are plotted with respect to KE. The KE and phytoplankton bloom relationship appears to hold across the broader Drake Passage during the observational period.

At low mesoscale kinetic energy, stratification and the vertical structure of the ocean is ordered by hydrostatic equilibrium. However baroclinic instabilities that change the vertical structure of the ocean can occur at high mesoscale kinetic energies. Here we consider five-day averaged kinetic energy (KE) in the upper 30 m of the water column. The KE was computed using NOAA OSCAR currents and estimated at the float locations (see Materials and Methods). NOAA OSCAR currents resolve mesoscale dynamics resulting from geostrophic motion caused by sea surface height anomalies and ageostrophic motion caused by wind-driven circulation and temperature gradients[25].

Figure (3a) is the temporal progression of the column integrated chlorophyll-a concentration above z_c ($[Chl]|_c$) with respect to KE over the bloom-export period. Figure (3b) shows vertical $[Chl]$ profiles at key times during the bloom and export. The progression begins on DOY 73 with moderate KE (475 cm s^{-2}) and low $[Chl]|_c$ (136 mg m^{-2}). As the bloom grew, KE decreased by 77% to 109 cm s^{-2} on DOY 85, while $[Chl]|_c$ more than doubled to 359 mg m^{-2}. The MLD and z_c appear unchanged by the KE below 400 cm^{2}s^{-2} indicating that the vertical structure of the water column was not sensitive to low KE (Figure 3c). We interpret this as a mesoscale analog to the formation of blooms during reduced turbulent mixing[7].

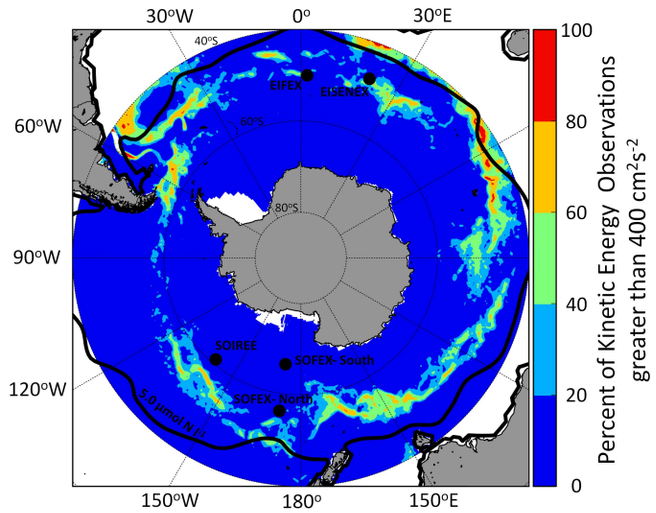

Fig. 5. The percent of NOAA OSCAR five-day averaged kinetic energy observations greater than 400 $cm^2\,s^{-2}$ in austral summer (December, January, and February) between 2004–2013. The black contour shows the climatological location of the 5 μmol l^{-1} surface nitrate (N) concentration contour during austral summer[37]. SO locations south of the 5 μmol N l^{-1}, and where the percentage of kinetic energy observations $>$ 400 $cm^2\,s^{-2}$ si high, may be unsuitable for large-scale iron additions as a means of enhancing the biological pump. Also shown are the locations of SO iron fertilization experiments: SOIREE[12], EISENEX[20], SOFEX-South and -North[21], and EIFEX[22].

During peak bloom (DOY 85–89), the $[Chl]|_c$ in each profile was greater than 350 mg m^{-2}. For comparison, the average $[Chl]|_c$ during the observational period was 147 mg m^{-2} with a standard deviation of $\pm$ 69 mg m^{-2}. The KE continued to decrease to 55 $cm^2\,s^{-2}$ on DOY 89 with a well defined surface phytoplankton bloom (Figure 3b). The net growth rate for $[Chl]|_c$ between subsequent profiles ($\Delta t = t_1 - t_0$) are estimated by

$$r = \frac{\ln\left([Chl]|_{c_1}\right) - \ln\left([Chl]|_{c_0}\right)}{\Delta t}. \qquad [1]$$

The estimated net growth rates were generally less than 0.1 day^{-1}, which is within the observed ranges[12].

The averaged chlorophyll-a concentration above z_c ($<[Chl]>_c$) during the peak bloom was $\sim$ 2.0 mg m^{-3}. By applying known carbon-to-chlorophyll[22] and carbon-to-iron ratios[26] in the SO (see Materials and Methods), we estimate the naturally occurring bloom would have required $\sim$ 0.19 nmol Fe l^{-1} which is comparable with observed dissolved iron concentrations in the Drake Passage[27]. This suggests that the bloom is not a result of a foreign iron injection.

After the peak bloom, $[Chl]|_c$ decreased by 42% between DOY 89–93 while KE remained below 62 $cm^2\,s^{-2}$ (Figure 3a). The vertical $[Chl]$ profiles (Figure 3b) appear to indicate the $[Chl]$ loss is uniform with depth in the surface ocean. Backscatter also reduced in a similar manner (Figure S3), indicating that the change in $[Chl]|_c$ in Figure (3a) was not due to changes in intracellular pigment concentrations. Furthermore, Figure (2a) does not show organic carbon export into the deep ocean between DOY 89–93. Our interpretation is that the prolonged low KE allowed a grazing ecosystem to organize around the concentrated phytoplankton bloom which is a mesoscale analog to seasonal ecosystem re-coupling of grazing pressure[28].

Export Sequence. Our observations suggest that bloom development is predicated on increasing phytoplankton residence time in the euphotic layer due to low KE, however the mechanisms driving organic carbon export are different. Between DOY 93–105, the $[Chl]|_c$ remained fairly constant (Figure 3a) with a decrease of only 16%. The KE increased by over an order of magnitude from 62 to 1,045 $cm^2\,s^{-2}$ and z_c deepened from 175 to 289 m indicating that increased KE was sufficiently strong to alter the vertical structure of the water column (Figures 3a,c). This suggests that the post-grazed phytoplankton bloom is being diluted as z_c deepens (Figure 3a,b).

Phytoplankton export to the deep ocean occurred from DOY 101–109 while the KE remained high and z_c continued to deepen. In Figure (2a), the $[Chl]$ spikes deeper in the water column between DOY 101–109 coincide with spikes in the particle backscatter coefficient (b_{bp}, Figure S1c). This suggests that the deep $[Chl]$ features are associated with aggregated phytoplankton[29] that rapidly sink out of the surface ocean[30]. We estimated a sinking rate of 125 m day^{-1} (see Materials and Methods) between DOY 103–105 which is comparable with other particle flux studies[31].

Given that aggregated phytoplankton sink until reaching their neutral density points, the KE-driven deepening of z_c and other isopycnals played a role in deepening phytoplankton biomass. Therefore, under high KE cell aggregates of a particular density are deeper in the water column than expected under a lower KE regime (Figures 2a, 3b), thus priming the system for deep ocean particle export. During the export event, the MLD remained essentially unchanged (Figure 2b); therefore it appears that the KE-driven deepening of isopycnals (and the neutral density points of cell aggregates) is more important than MLD for phytoplankton export.

Kinetic Energy and Bloom Relationship. Biofloat observations during the bloom-export period suggest low KE regimes lead to bloom formation. However, our analysis of all biofloat $[Chl]|_c$ and KE measurements during the observation period (Figure 4a) indicates low KE is a necessary, but not sufficient condition for bloom formation. Low levels of KE do not appear strong enough to impact the vertical structure of the surface ocean water column (Figure 3c), potentially allowing for increased residence time within the well-lit euphotic layer [7, 8]. However, blooms are not always present during low KE as other limiting factors still exist [10, 19].

The in-situ relationship between KE and bloom formation (Figure 4a) creates an expectation that satellite observations of phytoplankton blooms should be more probable during low KE regimes. To test this expectation, we examined coincident estimates of satellite observed chlorophyll-a concentration and OSCAR KE (see Materials and Methods) across the entire Drake Passage during the observational period (Figure 4b). We conclude that the relationship between mesoscale kinetic energy and bloom formation observed by the biofloat is characteristic of the entire Drake Passage. Our observations are opposite of what is expected in North Atlantic Gyre (and most sub-tropical systems) where higher levels of kinetic energy are required to mix limiting nutrients into the euphotic layer [32].

No blooms were observed in our in-situ observations (Figure 4a) or satellite analysis (Figure 4b) during high KE regimes. This suggests that residence time in the euphotic zone is a primary limiting factor for naturally occurring phytoplankton blooms, which is contrary to studies that use MLD as a proxy for light limitation[33]. Our biofloat observations show the MLD remained fairly constant during the observational period and did not correlate with $[Chl]$ (Figure S4). This suggests the MLD could be the wrong parameter for evaluating the importance of light on bloom formation. Furthermore, SO

blooms have generally only been observed where stratification provides a favorable light regime, even when iron is naturally in excess[34].

While iron concentration are decidedly low across much of the SO [10, 11], our analysis suggests that low KE is a necessary precondition for bloom formation. Since successful iron addition experiments[12, 20, 21, 22, 23] were conducted in generally low KE environments (Table S1), it is possible that the general experimental design of iron addition occludes KE as a major controlling factor of phytoplankton bloom formation in the SO.

Furthermore, if high levels of mesoscale kinetic energy impose a significant limitation on phytoplankton abundance across the SO, there may be regions of the energetic SO unsuitable for geoengineered draw down of atmospheric CO_2 through large scale iron injections. Our results indicate that the vertical structure of the surface ocean water column is unchanged by KE below $400\,\mathrm{cm^2\,s^{-2}}$ (Figure 3c) and, accordingly, phytoplankton abundance is generally suppressed above it (Figure 4) . Therefore, we take $400\,\mathrm{cm^2\,s^{-2}}$ as an approximate threshold between favorable (low KE) and unfavorable (high KE) phytoplankton regimes in the SO. Figure (5) shows the percent of five-day averaged kinetic energy observations above $400\,\mathrm{cm^2\,s^{-2}}$ during the austral summer from 2004-2013. Also plotted is the climatological location of the $5\,\mu\mathrm{mol\,l^{-1}}$ surface nitrate (N) concentration contour during austral summer[37]. Regions south of this contour are characterized by high nitrate and low chlorophyll concentrations in the surface ocean where limited iron availability often prohibits phytoplankton growth. We assert that regions of the SO south of the $5\,\mu\mathrm{mol\,N\,l^{-1}}$ contour, and where the percentage of kinetic energy values above $400\,\mathrm{cm^2\,s^{-2}}$ is high, may be unsuitable for large-scale iron fertilization experiments.

Conclusions

In conclusion, a biofloat profiling the Drake Passage every other day has provided an unprecedented look at the temporal development of a naturally occurring phytoplankton bloom, and subsequent organic carbon export into the deep ocean. Our analysis shows that low levels of mesoscale kinetic energy are a necessary pre-condition for natural bloom formation in the Southern Ocean before other potentially limitation factors (e.g. micronutrients, grazing relaxation) can be considered. Furthermore, high levels of mesoscale kinetic energy may limit phytoplankton bloom develop in the SO and, when preceded by a bloom, appear to facilitate carbon export into the deep ocean.

Materials and Methods

Biofloat and Surface Current Tracers.

Our analysis and interpretation of observations during the bloom-export event is predicated on the notion that the biofloat, profiling the water column every two days, acts as a near-Lagrangian tracer with respect to the surface ocean motion. The biofloat trajectory during the bloom-export period is compared with surface tracer trajectories computed using the NOAA OSCAR five-day averaged currents estimated at the biofloat locations (see below). The u and v current components at the biofloat locations are used to project the likely tracer trajectories over the course of two days. Figure (S2) shows that the biofloat acts as a near-Lagrangian tracer with respect to motion in the surface ocean.

Biofloat Data Analysis.

The biofloat instrument payload included a SeaBird model 41 CTD and a WET Labs Combination Fluorometer-Scattering-CDOM Sensor. Measurements were made at discrete sampling depths during ascent to the surface. Below 1,000 dbar measurements were made every 100 dbar, between 1,000 and 500 dbar measurements were made every 50 dbar, and above 500 dbar measurements were made every 5 dbar for a high resolution sampling of the upper ocean. Pressure is converted to depth by assuming hydrostatic balance with a standard atmosphere of pressure at the ocean surface. Density is calculated following Gill[35].

Profiles of temperature, salinity, particle backscatter coefficient and colored dissolved organic matter are shown in Figures (S1a-d). One profile (DOY 71) was eliminated from the analysis because it exhibited unrealistic and noisy density inversions. This may be due to a temporary blockage in the conductivity cell on that profile.

Characteristic Isopycnal.

We chose $\rho = 1027.45\,\mathrm{kg\,m^{-3}}$ as the characteristic isopycnal of the system because it tracked the bottom of the surface chlorophyll layer better than the mixed layer depth (MLD; taken as the depth of maximum $\partial\rho/\partial z$ in each smoothed vertical density profile). Chlorophyll concentrations in excess of $1\,\mathrm{mg\,m^{-3}}$ were consistently observed below the MLD. This is an expected result because MLD does not explicitly correspond to the neutral density of phytoplankton cells which determines their vertical location in the water column. Furthermore, we believe the characteristic isopycnal is highly correlated to other isopycnals and interlaces the relationship between mesoscale kinetic energy and vertical density structure. Neither the KE or depth of the characteristic isopycnal (z_c) are strongly correlated with MLD ($R^2 = 0.43$ and 0.39, respectively). When compared with temperature observations (Figure S1a), the MLD appears to track the top of the Antarctic Winter Water[36].

Daily Averaged Mean Kinetic Energy.

National Oceanic and Atmospheric Administration (NOAA) Ocean Surface Current Analysis–Real time (OSCAR) currents were computed by combining a quasi-steady geostrophic model (derived from altimetry) with wind-driven ageostrophic currents and thermal wind adjustments. The currents are depth averaged to 30 meters (see Bonjean $et\ al.$[25] for full model description). The 1/3°resolution, five-day averaged surface current product we used is available at http://www.oscar.noaa.gov/.

The data product comes as discrete, temporal blocks of five-day averaged currents . We further process the OSCAR currents by assuming each block only represents the daily, five-day averaged current field (u_{daily} and v_{daily}) on the centered date. We linearly interpolated the five-day averaged currents to each day of the year. The daily, five day averaged kinetic energy at each grid point is

$$KE_{daily} = \frac{1}{2}\left(u_{daily}^2 + v_{daily}^2\right). \qquad [2]$$

KE_{daily} is bi-linearly interpolated spatially to locations on Earth (KE) using a sphere.

Bloom Required Dissolved Iron Estimate.

During peak bloom, we observed a maximum $<[Chl]>_c$ of $\sim 2.0\,\mathrm{mg\,m^{-3}}$. From Figure (5b) in Hoffmann et $al.$[22] we chose a carbon-to-chlorophyll ratio of $\sim 25\,\mathrm{g\,C}$ to $1\,\mathrm{g\,Chl}$. This value appropriately represents the measured ratios for the largest eukaryotic cells analyzed (3.9 μm), just after iron fertilization. Furthermore, from Figures (1) and (2) in Twining et $al.$[26] we chose a carbon-to-iron ratio $\sim$ 45 μmol Fe to 1 mol C. This value generally reflects their measured ratios for diatoms. Therefore we roughly estimate the iron required during the peak bloom was:

$$\frac{2\,\mu\mathrm{g\,Chl}}{\mathrm{l}} \times \frac{1\,\mathrm{g\,Chl}}{1,000,000\,\mu\mathrm{g\,Chl}} \times \frac{25\,\mathrm{g\,C}}{1\,\mathrm{g\,Chl}} \times \frac{1\,\mathrm{mol\,C}}{12\,\mathrm{g\,C}} \times \frac{45,000\,\mathrm{nmol\,Fe}}{1\mathrm{mol\,C}} \approx 0.19\,\frac{\mathrm{nmol\,Fe}}{\mathrm{l}}. \qquad [3]$$

Five Day Composite Surface Chlorophyll Concentrations.

Daily, 9 km level 3 Moderate Resolution Imaging Spectroradiometer (MODIS) Aqua satellite $[Chl]$ data was downloaded from http://oceancolor. gsfc.nasa.gov between January 10 and June 4, 2013. The data was subset to the three spatial boxes in Figure S5 that represent the greater Drake Passage. Five day surface chlorophyll-a composites were made corresponding to each of the five-day averaged NOAA OSCAR data blocks processed.

Sinking Rates.

Sinking rates are determined by changes in the deepest extent of twenty evenly spaced iso-chlorophyll lines between 0.1 - 0.4 mg m^{-3}. The vertical change (Δz) between two filtered profiles (Δt) gives the sinking rate ($\Delta z/\Delta t$). The twenty sinking rates are depth averaged for one estimate of vertical motion between two filtered profiles.

ACKNOWLEDGMENTS. This research was funded by the Charles and Patricia Robertson Research Fund and Graduate Fellowship. A.R.D. would like to thank Pablo Huq, Robert Vaillancourt, and Mark Moline for constructive discussion. A.R.D. would like to thank Scott Davies for compiling Movie S1. The authors would like to thank Joseph Brodie and Dana Veron for manuscript review.

1. Ciais P, et al. (2013) Carbon and Other Biogeochemical Cycles. In: Climate Change 2013: The Physical Science Basis. Contribution of Working Group I to the Fifth Assessment Report of the Intergovernmental Panel on Climate Change, eds Stocker TF, Qin D, Plantter G-K, Tignor M, Allen SK, Boschung J, Nauels A, Xia Y, Bex V, Midgley PM (Cambridge, United Kingdom and New York, NY, USA.) pp 530–531.
2. Falkwoski PG, Ziemann D, Kolber Z, Bienfang P (1991) Role of eddy pumping in enhancing primary production in the ocean. Nature 352:55–58.
3. McGillicuddy DJ, et al. (1998) Influences of mesoscale eddies on new production in the Sargasso Sea. Nature 394:263–266.
4. Hense I, Bathmann UV, Timmermann R (2000) Plankton dynamics in frontal systems of the Southern Ocean. Journal of Marine Systems 27:235–252.
5. Klein P, Lapeyre G (2009) The Oceanic Vertical Pump Induced by Mesoscale and Submesoscale Turbulence. Annual Review of Marine Science 1:351– 375.
6. Huisman J, van Oostveen P, Weissing F (1991) Critical depth and critical turbulence. Limnology and Oceanography 44:1781–1787.
7. Taylor JR, Ferrari R (2011) Shutdown of turbulent convection as a new criterion for the onset of spring phytoplankton blooms. Limnology and Oceanography 56:2293–2307.
8. Sverdrup HU (1953) On conditions for the vernal blooming of phytoplankton. Journal du Conseli International pour l'Exploration de la Mer 18:287–295.
9. Behrenfeld M (2010) Abandoning Sverdrup's Critical Depth Hypothesis on phytoplankton blooms. Ecology 91:977–989.
10. Martin JH (1990) Glacial-interglacial CO_2 change: The Iron Hypothesis. Paleoceanography 5:1–13.
11. Martin JH, Gordon RM, Fitzwater SE (1990) Iron in Antarctic waters. Nature 345:156–159.
12. Boyd PW, et al. (2000) A mesoscale phytoplankton bloom in the polar Southern Ocean stimulated by iron fertilization. Nature 407:695–702.
13. Takahashi T, et al. (2002) Global sea-air flux based on climatological surface ocean pCO_2 and seasonal biological and temperature effects. Deep-Sea Research II 49:1601–1622.
14. McNeil BI, Metzl N, Matear RJ, Corbiere A (2007) An empirical estimate of the Southern Ocean air-sea CO_2 flux. Global Biogeochemical Cycles 21:BG3011.
15. IPCC (2013) Summary for Policymakers. In: Climate Change 2013: The Physical Basis. Contribution of Working Group I to the Fifth Assessment Report of the Intergovernmental Panel on Climate Change eds Stocker TF, Qin D, Plantter G-K, Tignor M, Allen SK, Boschung J, Nauels A, Xia Y, Bex V, Midgley PM (Cambridge University Press, Cambridge, United Kingdom and New York, NY, USA).
16. Sarmiento JL, Hughes TMC, Stouffer RJ, Manade S (1998) Simulated response of the ocean carbon cycle to anthropogenic climate warming. Nature 393:245–249.
17. Moore JK, Abbott MR (2000) Phytoplankton chlorophyll distributions and primary production in the Southern Ocean. Journal of Geophysical Research 105:28709–28722.
18. Arrigo KR, van Dijken GL, Bushinsky S (2008) Primary production in the Southern Ocean, 1997–2006. Journal of Geophysical Research 113:C08004.
19. El-Sayed S (1987) Productivity of the Antarctic Waters–A Reappraisal. In: Marine Phytoplankton and Productivity eds Holm-Hansen O, Bolis L, Gilles R (Springer Berlin Heidelberg, Germany). pp 19–34.
20. Gervais F, Riebesell U, Gorbunov MY (2002) Changes in primary productivity and chlorophyll a in response to iron fertilization in the Southern Polar Frontal Zone. Limnology and Oceanography 47:1324–1335.
21. Coale KH et al. (2004) Southern Ocean Iron Enrichment Experiment: Carbon Cycling in High- and Low-Si Waters. Science 304:408–414.
22. Hoffmann LJ, Peeken I, Lochte K, Assmy P, Veldhuis M (2006) Different reactions to Southern Ocean phytoplankton size classes to iron fertilization. Limnology and Oceanography 51:1217–1229.
23. Smetacek V et al. (2012) Deep carbon export from a Southern Ocean iron-fertilized diatom bloom. Nature 487:313–319.
24. Daniault N, Menard Y (1985) Eddy Kinetic Energy Distribution in the Southern Ocean From Altimetry and FGGE Drifting Buoys. Journal of Geophysical Research 90:11877–11889.
25. Bonjean F, Lagerloef GSE (2002) Diagnostic Model and Analysis of the Surface Currents n the Tropical Pacific Ocean. Journal of Physical Oceanography 32:2938–2954.
26. Twining BS, Baines SB, Fisher NS, Landry MR (2004) Celluar iron contents of plankton during the Southern Ocean Iron Experiment (SOFeX).Deep-Sea Research I 51:1827–1850.
27. Klunder MB, et al. (2014) Dissolved Fe across the Weddell Sea and Drake Passage: impacts of DFe on nutrient uptake. Biogeosciences 11:651–669.
28. Behrenfeld MJ, Boss ES (2014) Resurrecting the Ecological Underpinnings of Ocean Plankton Blooms. Annual Review of Marine Science 6:167–194.
29. Briggs N, et al. (2011) High-resolution observations of aggregate flux during a subpolar North Atlantic spring bloom. Deep-Sea Research II 58(10):1031–1039.
30. Turner JT (2002) Zooplankton fecal pellets, marine snow and sinking phytoplankton blooms. Aquatic Microbial Ecology 27:57–102.
31. Fischer G, Karakas G (2009) Sinking rates and ballast composition of particles in the Atlantic Ocean: implications for the organic carbon fluxes of the deep ocean. Biogeosciences 6:85–102.
32. Oschlies A, Garcon V (1998) Eddy-induced enhancement of primary production in a model of the North Atlantic Ocean. Nature 394:266–269.
33. Venables V, Moore MC (2010) Phytoplankton and light limitation in the Southern Ocean: Learning from high-nutrient, high-chlorophyll areas. Journal of Geophysical Research: Oceans 115:C02015.
34. Mitchell BG, Brody EA, Holm-Hansen O, McClain C, Bishop J (1991) Light limitation of phytoplankton biomass and macronutrient utilization in the Southern Ocean. Limnology and Oceanography 36:1662–1677.
35. Gill AE (1982) Appendix 3: Properties of Seawater In: Atmosphere–Ocean Dynamics (Elsevier Science) pp 599-600.
36. Toole JM (1981) Sea Ice, Winter Convection, and Temperature Minimum in the Southern Ocean. Journal of Geophysical Research 86:8037–8047.
37. Garcia HE, et al. (2010) Nutrients (phosphate, nitrate, silicate). In: CWorld Ocean Atlas 2009, Volume 4, eds Levitus ED (NOAA Atlas NESDIS 71, U.S. Government Printing Office, Washington, D.C.) pp 398.